Optics Letters

Inverse design of a spatial filter in edge enhanced imaging

Xinlei Zhu,[1] Hainan Yao,[1] Jiayi Yu,[2] Greg Gbur,[3] Fei Wang,[1,4] Yahong Chen,[1,5] and Yangjian Cai[1,2,6]

[1]*School of Physical Science and Technology & Collaborative Innovation Center of Suzhou Nano Science and Technology, Soochow University, Suzhou 215006, China*

[2]*Shandong Provincial Engineering and Technical Center of Light Manipulation & Shandong Provincial Key Laboratory of Optics and Photonic Device, School of Physics and Electronics, Shandong Normal University, Jinan 250014, China*

[3]*Department of Physics and Optical Science, University of North Carolina at Charlotte, Charlotte, North Carolina 28223, USA*

[4]*e-mail: fwang@suda.edu.cn*

[5]*e-mail: yahongchen@suda.edu.cn*

[6]*e-mail: yangjiancai@suda.edu.cn*

A spatial filter, as a key element in edge enhanced imaging, determines the resolution and the contrast of imaging. However, the conventional spiral phase filter (SPF) results in background noise near the edges of objects in the formed images due to the fact that the point spread function (PSF) of the SPF has sub-oscillations that decrease the edge resolution. In this Letter, we propose a method for inversely designing the spatial filter, aiming to achieve high-resolution images. We show that the sub-oscillations in the PSF of the filter can be, in principle, completely suppressed. Further, we experimentally demonstrate the edge enhancement, with high resolution, for both amplitude and phase objects by using our own designed filter. Our method may find potential applications in fingerprint identification and image processing. © 2020 Optical Society of America

The technique of edge enhancement, which extracts the important information at the boundary of objects in optical imaging, has significant applications in many areas such as biological imaging [1,2], astronomical observation [3,4], fingerprint identification [5], and remote sensing [6]. Up to now, several approaches have been proposed to realize edge enhancement, including differential interference contrast [7,8], radial Hilbert transformation [9], and the use of metamaterials or plasmonic structures [10,11]. Among them, the radial Hilbert transformation is one of the most well-known and convenient methods to achieve an edge enhanced image. Such a method uses a spiral phase filter (SPF) in the Fourier transform plane of a $4f$ imaging system to filter the spatial frequency information, leading to a strong edge contrast for both amplitude and phase objects [9,12–14]. The SPF has further been embedded into the microscopy system for the observation of the phase contrast image of bio-tissues and cells [14–16]. Bernet and co-workers demonstrated quantitative imaging of a complex object reconstructed from at least three spatially filtered images through different rotational orientations of SPFs in phase contrast microscopy [17]. Recently, the SPF has been extended to nonlinear optics for advancing the concept of the nonlinear spiral phase contrast image [18].

Any straight line crossing the singular point of the SPF corresponds to a 1D Hilbert transformation. Therefore, the amplitude and phase contrast images by the SPF are isotropic, i.e., independent of their local orientations. In order to realize orientation-selective edge enhancement, the modified SPFs, such as the fractional SPF [19–21], the phase shifted SPF [22,23], and the SPF with spatial-varying polarization [24,25], are used to break the isotropy of the traditional one.

However, the conventional as well as the modified SPFs are not the optimal filters, since the superfluous side lobes, near the main lobe in the point spread function (PSF) of the SPF, give rise to diffraction noise near edges, decreasing the imaging resolution. To overcome this issue, the Laguerre–Gaussian SPF was proposed, instead of a conventional SPF, to suppress the side lobes in the PSF [13]. Later, a SPF with the Bessel-type amplitude was introduced to further reduce the diffraction noise [26]. More recently, it was demonstrated that an Airy SPF [27], compared with the aforementioned filters, may display some advantages in achieving an amplitude or phase contrast image with high resolution. Nevertheless, there is still a lack of good guidelines for designing an optimum filter for practical situations.

In this Letter, we advance an effective protocol for inversely designing the spatial filter in the Fourier plane of a $4f$ edge enhanced imaging system via PSF engineering. The inversely designed spatial filter makes the sub-oscillations in the PSF be totally suppressed, thus leading to a high quality of amplitude and phase contrast imaging. With the help of a spatial light modulator (SLM), we carry out experiments to demonstrate the edge detection, with high resolution, for both amplitude and phase objects by using our inversely designed spatial filter.

Typical edge enhanced imaging is based on the classical $4f$ system, as shown in Fig. 1, where (x_0, y_0), (u, v), and (x, y) are the Cartesian coordinates in the object plane, Fourier plane, and image plane, respectively. An object with (complex) transmittance $g(x_0, y_0)$ is illuminated by a collimated coherent light. The Fourier transform of the object $G(u, v)$ is formed in the rear focal plane (Fourier plane in Fig. 1) of L_1. A spatial filter with a (complex) transmission function $H(u, v)$ is located in the Fourier plane to modulate the spatial frequency information of the object. The output function $o(x, y)$ in the image plane is a Fourier transform of the product of functions $H(u, v)$ and $G(u, v)$. According to the convolution theorem, it takes on the form

$$o(x, y) = g(x, y) \otimes h(x, y), \tag{1}$$

where "$\otimes$" represents the convolution operation. The Fourier transform of the spatial filter $h(x, y)$ (also named PSF of the spatial filter) is given by

$$h(x, y) = \frac{i}{\lambda f} \iint H(u, v) \exp\left[-\frac{i2\pi}{\lambda f}(ux + vy)\right] \mathrm{d}u\mathrm{d}v, \tag{2}$$

where λ is the wavelength of the illumination, and f is the focal length of the lens.

The transmission function of the conventional SPF in a $4f$ edge enhanced imaging system is expressed as

$$H(\rho, \varphi) = \mathrm{circ}\left(\frac{\rho}{R}\right)\exp(i\varphi), \tag{3}$$

where (ρ, φ) are the polar coordinates of the Fourier plane. Here circ is a circular aperture function of radius R induced by the sharp-edge aperture of the filter. On substituting Eq. (3) into Eq. (2) and integrating over ρ and φ, we obtain the following expression of the PSF for the SPF [9]:

$$h(x, y) = -\frac{i\pi R}{2r}\left[H_0(\xi)J_1(\xi) - H_1(\xi)J_0(\xi)\right]\exp(i\theta), \tag{4}$$

where $r = \sqrt{x^2 + y^2}$, $\theta = \arctan(y/x)$, and $\xi = 2\pi Rr/\lambda f$. Here H_0 and H_1 are the Struve functions of orders zero and one, respectively, whereas J_0 and J_1 are the Bessel functions of the first kind and of orders zero and one, respectively. It can be seen from Eq. (4) that the PSF is a complex function. For the sake of simplicity, we now consider only objects that are of pure amplitude or pure phase type. Based on Eq. (1), the intensity distribution $I(x, y) = |o(x, y)|^2$ in the image plane therefore can be written as

$$I(x, y) = |g(x, y) \otimes \mathrm{Re}[h(x, y)]|^2$$
$$+ |g(x, y) \otimes \mathrm{Im}[h(x, y)]|^2, \tag{5}$$
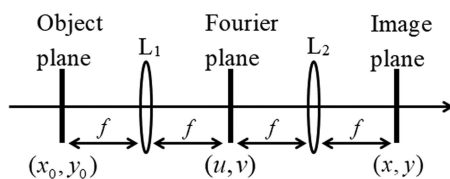
where Re and Im stand for taking the real and imaginary parts of a complex function, respectively.

It follows from Eq. (5) that the image captured by a detector in the image plane is a linear summation of the convolution of the object with the real part of the PSF and with the imaginary part of the PSF. In general, the variation of the PSF $h(x, y)$ with respect to variables x and y is much faster than that of $g(x, y)$, which means $g(x, y)$ is a slowly varying function with respect to $h(x, y)$. Thus, to obtain the best contrast of object edges in images, we require that the integral of the PSF over the whole space vanishes, i.e., $\iint h(x, y)\mathrm{d}x\mathrm{d}y = 0$. This condition implies that the transmission function $g(x, y)$ within a gradually varying region results in nearly zero intensity in the image plane, while within the region of sharp edges (rapid varying region), the received intensity is strongly enhanced. Such a condition is equivalent to the transmission function $H(u, v)$ of the filter being zero at the central point, i.e., $H(0, 0) = 0$. Therefore, for designing an optimal filter, the central point of the filter must be a singular point [9,12,26,27].

To further illustrate this process, we plot in Fig. 2 the contour graphs of the real and imaginary parts of the PSF of the SPF and the corresponding cross-lines in x and y directions, respectively. One finds that both the real and imaginary parts are composed of one positive and one negative peak, and a series of side lobes around them. Further, it is found that by rotating the imaginary part 90 deg clockwise, it becomes identical to the real part. From this characteristic, it is seen that the contributions to edge enhancement from the real and imaginary parts are "orthogonal," implying that the real part of PSF enhances the edge of the object only in x direction, whereas the y direction edge is enhanced only by the imaginary part.

By mimicking the vector representation, we may write the PSF in vector form as $\vec{h}(x, y) = \mathrm{Re}[h(x, y)]\hat{x} + \mathrm{Im}[h(x, y)]\hat{y}$, where $\hat{x}$ and $\hat{y}$ are two mutually orthogonal unit vectors in the x and y directions. For an object with sharp edges, it can be expressed as $\vec{t}(x, y) = t(x, y)\cos\phi\hat{x} + t(x, y)\sin\phi\hat{y}$, where $t(x, y)$ is the transmission function near the edge, and ϕ is the angle of the tangent line of the boundary with respect to the x axis. Thus, the image of the object boundary becomes

Fig. 1. Diagram of the $4f$ imaging system. Focal length of lenses L_1 and L_2 is f.
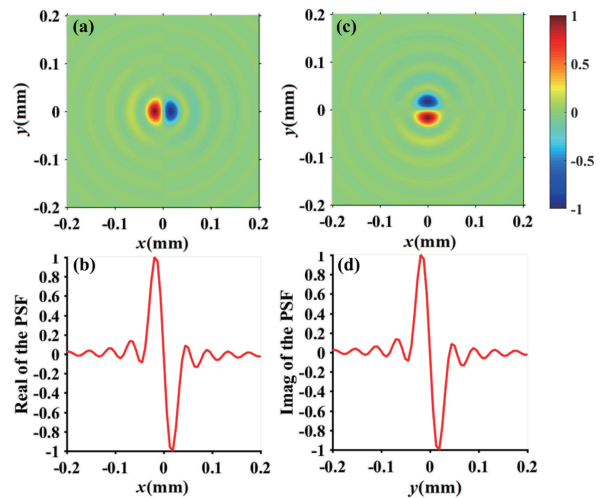
Fig. 2. (a), (c) Contour graphs of the real and imaginary parts of the PSF of the SPF; (b), (d) corresponding cross-lines of the real and imaginary parts in x and y directions, respectively.

$$I(x, y) = |t(x, y) \otimes \mathrm{Re}[h(x, y)]|^2 \cos^2 \phi$$
$$+ |t(x, y) \otimes \mathrm{Im}[h(x, y)]|^2 \sin^2 \phi. \quad \textbf{(6)}$$

Equation (6) is the main result of this Letter, which allows one to inversely design and optimize the spatial filter for achieving high quality of the edge enhanced image by starting from the PSF engineering. Note that Eq. (6) is valid only when the real and imaginary parts of the PSF are "orthogonal" to each other. Since the side lobes of the PSF of the spatial filter produce background noise in the image plane, one could re-shape the PSF, by using Eq. (6), to suppress the side lobes completely. One of the simplest forms for the PSF that is free of side lobes may be written as

$$h(x, y) = a[f(x + d_0, y) - f(x - d_0, y)]$$
$$+ ib[f(x, y + d_0) - f(x, y - d_0)], \quad \textbf{(7)}$$

where a and b are real coefficients, and d_0 is a shift parameter. The real function $f(x, y)$ is taken to have a single peak and can be, for instance, a Gaussian function, Lorentz function, or circular function. If the coefficients $a = b$, the edge enhancement image is isotropic; otherwise, it is anisotropic. Here, we notice that the corresponding transmission function $H(u, v)$ of the spatial filter, which can be obtained by the Fourier transformation of PSF $h(x, y)$ in Eq. (7), vanishes at the central point, i.e., $H(0, 0) = 0$.

For simplicity but without loss of generality, we assume that the function $f(x, y)$ is of Gaussian type, i.e.,

$$f(x, y) = \exp\left(-\frac{x^2 + y^2}{w_0^2}\right), \quad \textbf{(8)}$$

where w_0 is the width of the Gaussian function. We refer to the filter function with its PSF taking the form of Eq. (7) [Eq. (8) has been substituted] as the four-Gaussian filter (FGF). The real and imaginary parts of the PSF of the FGF are displayed in Figs. 3(a) and 3(b), respectively. In order to make the size of two peaks in Figs. 2(a) and 2(c) equivalent to Figs. 3(a) and 3(b), the parameters d_0 and w_0 are chosen to be 0.02 mm, while the parameters a and b are set as one. One can see in Figs. 3(a) and 3(b) that the PSF is free of side lobes. When performing the inverse Fourier transform of the PSF, the analytical expression for the transmission function of the FGF is found to be

$$H(u, v) = -\frac{2\pi w_0^2}{\lambda f} \exp\left[-\frac{\pi^2 w_0^2 (u^2 + v^2)}{\lambda^2 f^2}\right]$$
$$\times \left[\sin\left(\frac{2\pi u d_0}{\lambda f}\right) + i \sin\left(\frac{2\pi v d_0}{\lambda f}\right)\right]. \quad \textbf{(9)}$$

Figures 3(c) and 3(d) illustrate the amplitude and phase distribution of the filter function of FGF, respectively. It is found that the amplitude has rectangular symmetry, unlike that of the Laguerre–Gaussian SPF or Airy SPF, which are circular symmetric [13,27], and the phase shown in Fig. 3(d) is not a true spiral phase. However, when the argument in the sine function of Eq. (9) is smaller than 5 rad, i.e., $2\pi d_0 u(v)/\lambda f \le 5$ rad, the term in the second square brackets of Eq. (9) approximately reduces to $2\pi d_0 (u + iv)/\lambda f$, which is the form of a spiral phase. We also note here that we do not consider the aperture function $\mathrm{circ}(\rho/R)$ in the plane of the filter. Our numerical results (not shown here) show that the aperture function has almost no effect on our designed PSF if the radius R is larger than 5.0 mm. In principle, our filter has the best performance
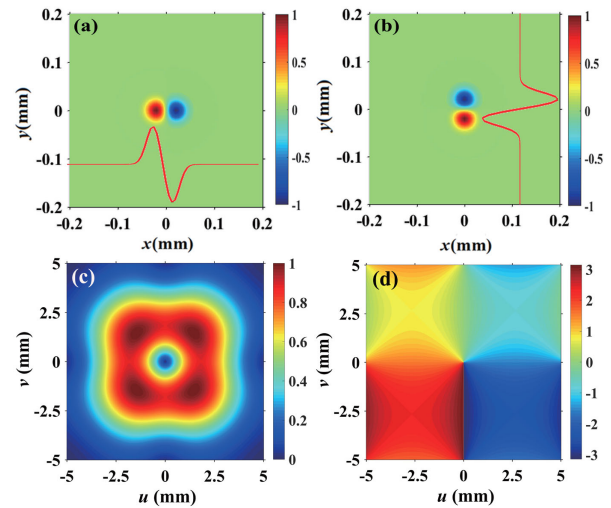
Fig. 3. (a), (b) Density plots of the real and imaginary parts, respectively, of the PSF shown in Eq. (7) when $f(x, y)$ is a Gaussian function in Eq. (8). (c), (d) Amplitude and phase distribution of the spatial filter function corresponding to the PSF in (a) and (b).

in edge enhanced imaging, since the side lobes in its PSF are suppressed completely.

We now carry out an experiment for edge enhanced imaging by using our inversely designed FGF and compare the results with those achieved by a conventional SPF. The experimental setup is shown in Fig. 4. A laser beam generated from a Nd:YAG laser ($\lambda = 532$ nm) passes through a neutral density filter (NDF) and a beam expander (BE), then goes toward the first SLM (SLM$_1$). Two lenses L$_1$ and L$_2$ with focal length $f = 400$ mm compose a typical $4f$ imaging system. The two SLMs SLM$_1$ and SLM$_2$ are located in the front and rear focal planes of L$_1$ acting as the object and the spatial filter, respectively. In the experiment, the circular apertures (not shown in Fig. 4) are separately placed in the optical path after SLM$_1$ and SLM$_2$ to filter out the first-order diffractions as desired object and spatial filter, respectively. The beam profile analyzer (BPA) is placed in the rear focal plane (i.e., image plane) of L$_2$. The inset figure in Fig. 4 is the computer generated hologram loaded by the SLM$_2$ to generate the inversely designed FGF.

A circular aperture with radius $R = 3.5$ mm is first used as an amplitude object to compare the edge enhanced images formed by the SPF and our inversely designed FGF. The transmission of
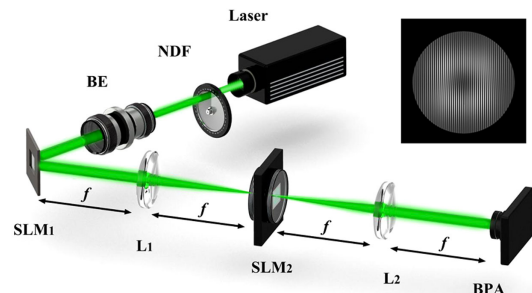
Fig. 4. Experimental setup for edge enhancement in a $4f$ imaging system. NDF, neutral density filter; BE, beam expander; SLM$_1$, SLM$_2$, spatial light modulators; L$_1$, L$_2$, lenses; BPA, beam profile analyzer. The inset is a computer generated hologram loaded by the SLM$_2$ to generate the inversely designed FGF.
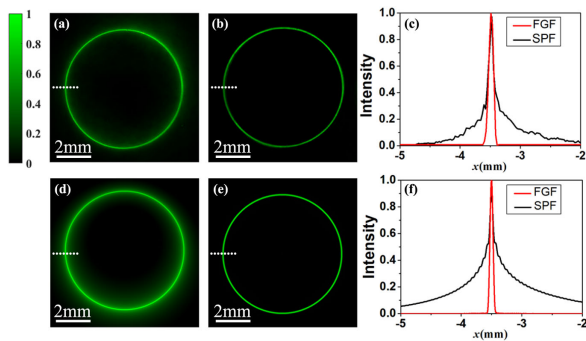
Fig. 5. (a), (b) Experimental results of the edge enhanced images of a circular aperture by means of (a) SPF and (b) FGF. (c) Corresponding 1D intensity distribution of the image along the dotted white lines. (d)–(f) Corresponding numerical simulation results.

the aperture for $R \leq 3.5$ mm is unity and zero for $R > 3.5$ mm. Figures 5(a) and 5(b) illustrate the experimental results of the recorded edge enhanced images by the SPF and the FGF, respectively. It is shown that the background noise near the edge has been effectively suppressed by using the FGF, in contrast to that using the SPF. To compare the detailed characteristics of the two images, Fig. 5(c) displays the cross-lines for intensity distributions at the edges denoted by dotted white lines in Figs. 5(a) and 5(b). It is seen clearly that the spatial resolution of the edge enhanced image is greatly improved when our FGF is adopted. For comparison, we plot in Figs. 5(d)–5(f) the corresponding numerical simulations. One finds that the experimental results agree well with the theoretical prediction.

Next, we examine the edge enhancement features of our FGF on a phase-only object. In this case, a panda phase picture [see Fig. 6(a)] is loaded by SLM_1 to act as the phase object. The edge enhanced images captured by the BPA with the SPF and the FGF are presented in Fig. 6(b) and 6(c), respectively. We find a high quality of the phase contrast image can also be achieved by adopting the inversely designed FGF, compared to that with the conventional SPF. We note that the intensity distribution on the edges is slightly inhomogeneous. This may be caused by the non-uniform intensity distribution of the illumination.

In conclusion, we have presented an approach for inversely designing the spatial filter used in a $4f$ edge enhancement optical system. The approach is based on engineering of the filter's PSF, completely suppressing its sub-oscillations. As a result, the high-contrast edge enhanced images with high resolution are obtained compared to those using a conventional SPF. Our approach can also be extended to design anisotropic (i.e., orientation-selective) edge enhancement by controlling a and b in Eq. (7). Moreover, the single peak function $f(x, y)$ in Eq. (8) can also be taken as a circular or a Lorentz-type function. By adjusting the function parameters appropriately, one may obtain edge enhanced imaging with much higher contrast/resolution. Due to the importance of edge enhancement of the phase objects (e.g., biological tissues), we will give more experimental examples of phase object edge enhancement with our inverse design method somewhere else.
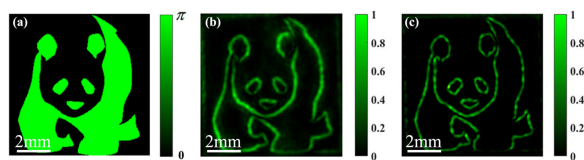
Disclosures. The authors declare no conflicts of interest.

REFERENCES

1. Z. Liu, L. Tian, S. Liu, and L. Waller, J. Biomed. Opt. **19**, 106002 (2014).
2. K. Haase, N. Kröger-Lui, A. Pucci, A. Schönhals, and W. Petrich, J. Biophoton. **9**, 61 (2016).
3. G. Foo, D. M. Palacios, and G. A. Swartzlander, Opt. Lett. **30**, 3308 (2005).
4. D. Mawet, E. Serabyn, J. K. Wallace, and L. Pueyo, Opt. Lett. **36**, 1506 (2011).
5. M. K. Sharma, J. Joseph, and P. Senthilkumaran, Opt. Laser Technol. **57**, 230 (2014).
6. G. Gibson, B. Sun, M. Edgar, D. Phillips, N. Hempler, G. Maker, G. Malcolm, and M. Padgett, Opt. Express **25**, 2998 (2017).
7. G. Nomarski, J. Phys. Radium **16**, 9 (1955).
8. T. J. McIntyre, Ch. Maurer, S. Bernet, and M. Ritsch-Marte, Opt. Lett. **34**, 2988 (2009).
9. J. A. Davis, D. E. McNamara, D. M. Cottrell, and J. Campos, Opt. Lett. **25**, 99 (2000).
10. T. Zhu, Y. Zhou, Y. Lou, H. Ye, M. Qiu, Z. Ruan, and S. Fan, Nat. Commun. **8**, 15391 (2017).
11. A. Pors, M. G. Nielsen, and S. I. Bozhevolnyi, Nano Lett. **15**, 791 (2014).
12. K. Crabtree, J. A. Davis, and I. Moreno, Appl. Opt. **43**, 1360 (2004).
13. C. Guo, Y. Han, J. Xu, and J. Ding, Opt. Lett. **31**, 1394 (2006).
14. S. Furhapter, A. Jesacher, S. Bernet, and M. Ritsch-Marte, Opt. Express **13**, 689 (2005).
15. C. Maurer, A. Jesacher, S. Fürhapter, S. Bernet, and M. Ritsch-Marte, J. Microsc. **230**, 134 (2008).
16. G. Situ, M. Warber, G. Pedrini, and W. Osten, Opt. Commun. **283**, 1273 (2010).
17. S. Bernet, A. Jesacher, S. Fürhapter, C. Maurer, and M. Ritsch-Marte, Opt. Express **14**, 3792 (2006).
18. X. Qiu, F. Li, W. Zhang, Z. Zhu, and L. Chen, Optica **5**, 208 (2018).
19. G. Situ, G. Pedrini, and W. Osten, J. Opt. Soc. Am. A **26**, 1788 (2009).
20. M. K. Sharma, J. Joseph, and P. Senthilkumaran, Appl. Phys. B **117**, 325 (2014).
21. J. Wang, W. Zhang, Q. Qi, S. Zheng, and L. Chen, Sci. Rep. **5**, 15826 (2015).
22. M. K. Sharma, J. Joseph, and P. Senthilkumaran, J. Opt. **42**, 1 (2013).
23. A. Jesacher, S. Furhapter, S. Bernet, and M. Ritsch-Marte, Phys. Rev. Lett. **94**, 233902 (2005).
24. B. Zhang, Z. Chen, H. Sun, J. Xia, and J. Ding, J. Opt. **18**, 035703 (2016).
25. B. S. B. Ram and P. Senthilkumaran, Opt. Lett. **43**, 1830 (2018).
26. S. B. Wei, S. W. Zhu, and X. C. Yuan, J. Opt. **13**, 105704 (2011).
27. Y. Zhou, S. Feng, S. Nie, J. Ma, and C. Yuan, Opt. Express **24**, 25258 (2016).

Fig. 6. (a) Phase object of a panda. (b), (c) Experimental results of edge enhanced images recorded by the BPA with SPF and FGF, respectively.